Nonlinear Schrödinger equation for integrated photonics

KEVIN BACH GRAVESEN[1,2,*] ASGER BRIMNES GARDNER[1,2] EMIL ZANCHETTA ULSIG[1,2], ERIC J. STANTON[3,4,5], MIKKEL TORRILD HANSEN[1], SIMON THORNDAHL THOMSEN[1], LUCAS AHLER[1], AND NICOLAS VOLET[1,2]

[1] Department of Electrical and Computer Engineering, Aarhus University, Aarhus, Denmark
[2] UVL A/S, Aarhus, Denmark
[3] EMode Photonix, Boulder, CO, USA
[4] Associate of the National Institute of Standards and Technology, Boulder, Colorado, USA
[5] Department of Physics, University of Colorado, Boulder, Colorado, USA
*kgr@uvmedico.com

Abstract: The foundations of nonlinear optics are revisited, and the formalism is applied to waveguide modes. The effect of loss and dispersion are included rigorously along with the vectorial nature of the modes, and a full derivation of a new version of the nonlinear Schrödinger (NLS) equation is presented. This leads to more general expressions for the group index, for the group-index dispersion (GVD), and for the Kerr coefficient. These quantities are essential for the design of waveguides suitable for e.g. the generation of optical frequency combs and all-optical switches. Examples are given using the silicon nitride material platform. Specifically, values are extracted for the coefficients of the chi-3 tensor based on measurements of Kerr coefficients and mode simulations.

1. Introduction

The nonlinear Schrödinger (NLS) equation has been a fundamental tool in photonics for decades [1], offering insights into dispersion and the behavior of light in nonlinear optical media. Its applications, spanning optical communications [2], frequency metrology [3], spectroscopy [4], ultrafast science [5], and quantum optics [6,7], underscore its paramount importance in modern optics. Today, the NLS equation is indispensable for modeling devices like all-optical switches [8,9] and optical parametric oscillation (OPO) [10,11]. These advancements in nonlinear optics have not only revolutionized chip-scale photonic capabilities but have also paved the path for breakthroughs in frequency synthesis [12], precision timing for positioning and navigation [13], frequency conversion of mid-infrared [14] to deep-UV [15] and a myriad of spectroscopic techniques [16].

Using the NLS equation, one can simulate how dispersion and nonlinearities affect the shape of an optical pulse as it propagates in a nonlinear medium [17]. The NLS equation is conventionally derived phenomenologically, inherited from bulk optics, and makes simplifying assumptions such as a lossless system and purely transverse fields [18,19]. However, for a guided mode in a material with loss, these assumptions may not necessarily be valid [20].

The NLS equation is here derived from first principles of Maxwell's equations in the special case of degenerate four-wave mixing [21]. The presented model avoids assumptions about polarization and the plane-wave approximation while accommodating discontinuities in the permittivity. This makes it universally applicable to all waveguides and especially well-suited for heterogeneous structures [22–24]. The NLS equation is typically derived assuming the existence of the optical Kerr effect [25], whereas in this work the Kerr effect follows directly from the NLS derivation. The bright soliton solution of the NLS equation is presented, from which a more general expression for the group index is found. The presented derivation of the Kerr effect differs from existing literature in the nonlinear phase shift being proportional to the optical power instead

of the intensity. This is a more relevant and convenient quantity in integrated photonics where the optical intensity in waveguides varies significantly over the cross-section. The presented model leads to a compact expression for the Kerr coefficient given by the third-order nonlinear tensor and the mode profile. As the waveguide modes are readily simulated in available software, it provides a powerful tool for optical engineers to better design nonlinear phase shifts. To indicate how the presented model differs from a conventional one, the third-order tensor element is found in silicon nitride using both models.

With the NLS equation being used as a tool to describe complicated optical effects and systems, we have included a detailed derivation in Supplement 1 to better be able to see where different terms and variables originate from. It also includes an example where the derived model is used to calculate Kerr coefficients in heterogeneous waveguides.

2. Chief equation and NLS equation

The complex wavenumber is expressed as:

$$k = \beta + i\alpha/2 = n\omega/c , \tag{1}$$

where β is the wavenumber, α the attenuation coefficient, n the effective refractive index of the relevant mode at the carrier frequency $\omega/(2\pi)$, and c is the speed of light in vacuum.

The complex electric field is decomposed as [26]:

$$\vec{\mathcal{E}} = e^{i\varphi} \mathcal{A}(z,t) \vec{e}(x,y) , \tag{2}$$

where $\varphi = kz - \omega t$. The complex vector $\vec{e}$ is the electric mode profile, which is independent of the longitudinal $\hat{z}$-direction. The complex function $\mathcal{A}$ is unitless and accounts for coupling between modes, as well as additional time dependencies. The fields are decomposed is terms of Fourier decomposition with the different Fourier frequencies $\Omega/2\pi$, not to be confused with the carrier frequency $\omega/(2\pi)$.

The modes are normalized with the following parameter [27]:

$$N \equiv \frac{1}{2} \iint_{\mathbb{R}^2} \left(\vec{e} \times \vec{\mathfrak{h}}^* \right) \cdot \hat{z} \, dx \, dy , \tag{3}$$

where $\vec{\mathfrak{h}}$ is the magnetic mode profile and the integration extends over the transverse plane of the waveguide. The mode profiles and the effective index are found by solving the dispersion relation [28], derived in Supplement 1, section 3. The chief equation involves the following quantity which depends on dispersion and the electric mode profile:

$$K(\Omega) \equiv \frac{1}{4\mu_0 \omega N} \iint_{\mathbb{R}^2} \gamma^2(\Omega) \, \vec{e} \cdot \vec{e}^* \, dx \, dy , \tag{4}$$

where μ_0 is the vacuum permeability, and the gamma factor γ is related to the material refractive index n_{mat} via:

$$\gamma(\Omega) = \Omega \, n_{\text{mat}}(\Omega)/c . \tag{5}$$

To explore how the K parameter relates to dispersion, it is Taylor expanded around ω:

$$K(\Omega) \approx K(\omega) + (\Omega - \omega)k_1 + \sum_{m=2}^{\infty} \frac{(\Omega - \omega)^m}{m!} k_m, \tag{6}$$

with:

$$k_1 \equiv \left. \frac{dK}{d\Omega} \right|_\omega , \quad k_m \equiv \left. \frac{d^m K}{d\Omega^m} \right|_\omega . \tag{7}$$

In the presence of dispersion, nonlinearity, and a finite value of attenuation, the $\mathcal{A}$ function is found by solving the chief equation:

$$\partial_z \mathcal{A} + k_1 \partial_t \mathcal{A} = T + i \sum_{m=2}^{\infty} k_m \frac{(i\partial_t)^2}{m!} \mathcal{A}. \tag{8}$$

The chief equation is derived directly from Maxwell's equations in Supplement 1, sections 2, 3 and 4. In the special case of continuous-wave (cw) operation, (8) reduces to the equation reported in [29].

The nonlinear interaction is accounted for in the term T:

$$T \equiv \frac{ie^{-i\varphi}}{4\omega N} \int_{-\infty}^{\infty} \Omega^2 e^{-i\Omega t} \iint_{\mathbb{R}^2} \left[\vec{\mathcal{P}}^{(\text{NL})}(\Omega) \cdot \vec{e}^* \, dx \, dy \right] d\Omega, \tag{9}$$

where $\vec{\mathcal{P}}^{(\text{NL})}$ is the Fourier component of the nonlinear polarization which depends on the nonlinear effects of interest. Looking at the self-induced effect of degenerate four-wave mixing, $\vec{\mathcal{P}}^{(\text{NL})}$ is found in Supplement 1, section 5 to be:

$$\vec{\mathcal{P}}^{(3)}(\Omega) = 3\varepsilon_0 \delta(\Omega - \omega) e^{-\alpha z} e^{ikz} \mathcal{A} |\mathcal{A}|^2 \, C\vec{v}. \tag{10}$$

ε_0 is the vacuum permittivity, C is the third-order nonlinear tensor that has been reduced by assuming Kleinmann symmetry [30] and $\vec{v}$ is a complex 10-row vector that involves the components of the electric mode profile. Both quantities are expanded on further in Supplement 1, section 6.

These quantities are used in the definition of a unitless coupling coefficient:

$$\kappa \equiv \frac{c\varepsilon_0}{4N} \iint_{\mathbb{R}^2} (C\vec{v}) \cdot \vec{e}^* \, dx \, dy. \tag{11}$$

For amorphous materials, the C tensor contains only one independent coefficient (c_{11}), resulting in a simplified integrand [31]:

$$(C\vec{v}) \cdot \vec{e}^* = \frac{c_{11}}{3} \left[(\vec{e} \cdot \vec{e})^2 + 2 (\vec{e} \cdot \vec{e}^*)^2 \right]. \tag{12}$$

Using (10) and (11) the nonlinear term (9) simplifies to:

$$T = i\Gamma e^{-\alpha z} \mathcal{A} |\mathcal{A}|^2, \tag{13}$$

where:

$$\Gamma \equiv 3\frac{\omega}{c}\kappa, \tag{14}$$

is defined to simplify notation and have units of m^{-1}. Inserting (13) into (8):

$$\partial_z \mathcal{A} + k_1 \partial_t \mathcal{A} = i\Gamma e^{-\alpha z} \mathcal{A} |\mathcal{A}|^2 + i \sum_{m=2}^{\infty} k_m \frac{(i\partial_t)^m}{m!} \mathcal{A}. \tag{15}$$

Relation (15) is a more general version of the nonlinear Schrödinger equation [32] that rigorously includes loss and the full vectorial nature of the modes. This contrasts with derivations found in textbooks where the longitudinal component of the electric field is neglected, and where the system is assumed lossless.

2.1. Temporal solitons

In the case where $k_m = 0$ for $m > 2$, the following function is an exact solution to (15):

$$\mathcal{A}(z, t) = \mathcal{A}_0 e^{Gz} \Big/ \cosh\left(\tau/\tau_0\right), \tag{16}$$

with the retarded time $\tau \equiv t - k_1 z$, a complex amplitude $\mathcal{A}_0$, a characteristic time τ_0 and a complex phase G. These parameters must satisfy the following conditions:

$$|\mathcal{A}_0|^2 = -\frac{k_2}{\Gamma \tau_0^2}, \tag{17}$$

and:

$$G = -i \frac{k_2}{2\tau_0^2}. \tag{18}$$

A pulse given by (16) does not vary in shape and is known as a temporal soliton [33–35].

The group velocity is defined as the speed of a pulse envelope. From (16) and the definition of τ, it is clear that k_1 is related to the group velocity v_g by:

$$k_1 = 1/v_g. \tag{19}$$

From (7) it is seen that k_2 then relates to the group-velocity dispersion (GVD). Equation (17) imposes that the sign of k_2 should be opposite to the sign of κ (seen from (14)). For bright solitons, a negative k_2 results in anomalous dispersion, and a positive κ [36]. If there is zero attenuation, these conditions also imply that τ_0 is real. Hence, τ_0 represents the temporal width of the pulse. Relation (16) is shown to solve (15) in Supplement 1, section 8.
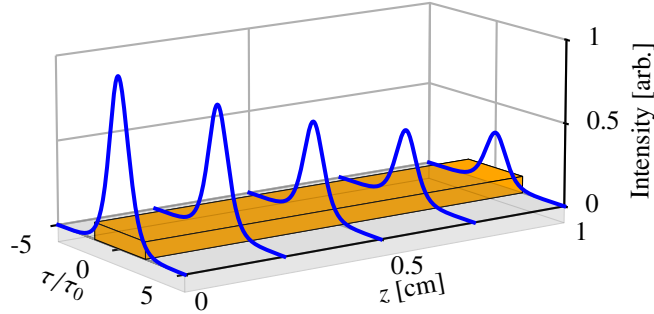

Fig. 1. Equation (16) plotted at different z as it propagates through a ridge waveguide with an attenuation of 5 dB/cm. The shape of the soliton doesn't change as it propagates but its intensity decreases due to loss.

2.2. Group index

From (7) and (19), the group index can be found from:

$$n_g \equiv c/v_g = c \left. \frac{\mathrm{d}K}{\mathrm{d}\Omega} \right|_\omega. \tag{20}$$

This expression seems to be more general than the common expression [37]:

$$\bar{n}_g = n + \omega \frac{dn}{d\omega}. \tag{21}$$

To compare n_g and $\bar{n}_g$, simulations were made of Si_3N_4 and GaAs waveguides enclosed in SiO_2 cladding. The relative error:

$$\epsilon \equiv (\bar{n}_g - n_g) / \bar{n}_g, \tag{22}$$

is then found and can be seen in Figure 2. As the waveguide thickness increases, so does the mode confinement, converging towards a homogeneous waveguide. The simulations are made with a 2 µm wide waveguide and a varying thickness (the Si_3N_4 waveguide is not simulated with a thickness below 100 nm, as the mode becomes highly unconfined). Values found from (21) are in general higher with a finite difference found in the third digit, showing an excellent match between the two expressions. The common expression (21) has been found to match well experimentally [38], giving us confidence in the validity of the presented formalism.
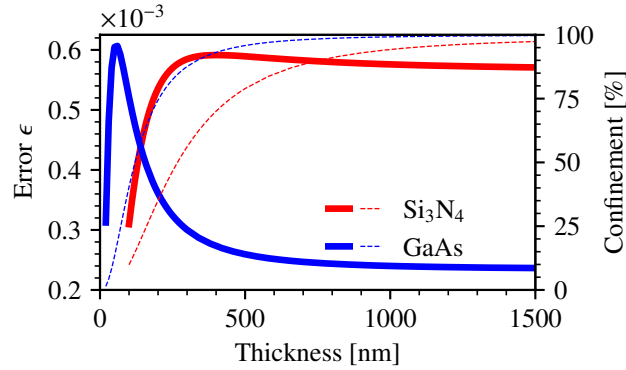

Fig. 2. Relative error (22) between the general expression (20) and the common expression (21) for the group index. Simulations are performed for a Si_3N_4 waveguide (in red) and a GaAs waveguide (in blue) as a function of the core thickness. Dashed lines show the confinement factor.

3. Optical Kerr effect

An important implication of the NLS equation is the optical Kerr effect. Under continuous-wave (cw) excitation, the NLS equation (15) reduces to:

$$\partial_z \mathcal{A} = i\Gamma e^{-\alpha z} \mathcal{A} |\mathcal{A}|^2. \tag{23}$$

The complex $\mathcal{A}$ function can be expressed as:

$$\mathcal{A} = e^{i\phi} A, \tag{24}$$

with a phase ϕ and a norm A, such that:

$$\partial_z \mathcal{A} = e^{i\phi} (\partial_z A + i A \partial_z \phi). \tag{25}$$

It can be deduced that $\partial_z A = 0$ (see Supplement 1, section 9). Using the expression for the optical power:

$$P = N e^{-\alpha z} A^2, \tag{26}$$

one finds:

$$\partial_z \phi = \frac{\Gamma}{N} P, \tag{27}$$

with Γ from (14). The third-order nonlinearity induces a phase change known as the optical Kerr effect. One further defines a change of effective index by:

$$\Delta n \equiv \frac{c}{\omega} \partial_z \phi = n_2 P, \tag{28}$$

with the Kerr coefficient:

$$n_2 \equiv 3\kappa/N . \tag{29}$$

Note that (28) is proportional to the power. This contrasts the classical result from bulk optics where the optical Kerr effect induces a change of material refractive index proportional to the intensity.

For a waveguide based on amorphous materials, (12) applies, and if there is only a negligible nonlinear contribution from the cladding, the coupling coefficient (11) reduces to:

$$\kappa = \frac{c\varepsilon_0}{12N} c_{11} \Sigma, \tag{30}$$

where:

$$\Sigma \equiv \iint_{\mathbb{R}^2} (\vec{e} \cdot \vec{e})^2 + 2 (\vec{e} \cdot \vec{e}^*)^2 \, dx \, dy . \tag{31}$$

The Kerr coefficient can then be expressed as:

$$n_2 = \frac{c\varepsilon_0}{4N^2} c_{11} \Sigma. \tag{32}$$

Using the mode profile to calculate a nonlinear effective refractive index has already been reported, e.g. in [39], but the presented formalism expands on this by being a direct consequence of the NLS equation, and not the other way around.

3.1. Third-order nonlinear coefficient

The c_{11} tensor element of amorphous Si_3N_4 is here found using multiple previous studies on the Kerr effect in Si_3N_4 waveguides. The chosen studies all measure the Kerr value in Si_3N_4 waveguides but have different cladding materials and geometries. Waveguides made from Si_3N_4 was chosen because it is an amorphous material for which (32) is applicable, it has a high third-order nonlinearity [40], has low loss with a broad transparency range [41] and is well used for a wide variety of third-order effects, especially frequency combs [42, 43].

In the conventional formalism the tensor element for an amorphous material can be found from a measured Kerr coefficient $\bar{n}_2$, with units $[m^2/W]$, by [19]:

$$\bar{c}_{11} = \bar{n}_2 n^2 \varepsilon_0 c \big/ 3 . \tag{33}$$

The Kerr coefficient $\bar{n}_2$ from the conventional formalism can be converted to the presented formalism by:

$$n_2 = \bar{n}_2/A_{\text{eff}} , \tag{34}$$

with A_{eff} being the effective mode area.

The waveguide structures investigated are either a Si_3N_4 waveguide embedded by SiO_2 cladding [40, 41] or a substrate of SiO_2 with a Si_3N_4 waveguide embedded and air cladding on top [44]. With heterogeneous structures, and n_2 given by (29), the transverse integral in κ is split
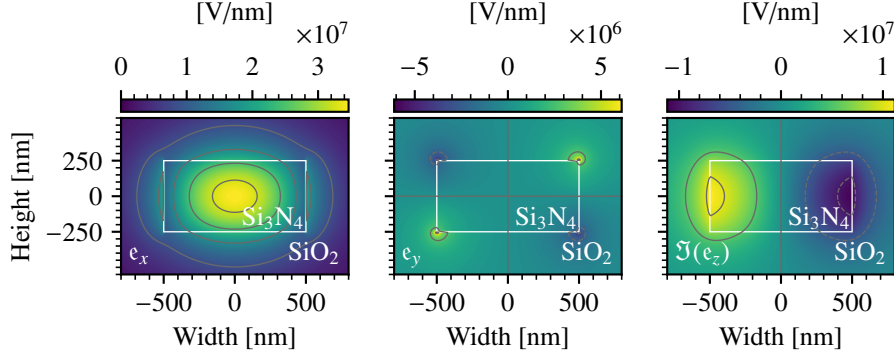
Fig. 3. Fundamental TE mode simulated at 1550 nm for a Si_3N_4 waveguide embedded in SiO_2. The waveguide core is 1000 nm wide and 500 nm thick, replicating the structure from [40]. The x and y components of the electric mode profile, $\vec{e}$, are purely real, with the z component being purely imaginary. The non-zero imaginary z component is visualized, motivating the derivation of the NLS equation without assuming this to be zero. The contour lines indicate a drop of 25%.

Table 1. c_{11} Calculation.

Study	Waveguide confinement	$10^{-19}\,\bar{n}_2$ [m²/W]	$10^{-21}\,\bar{c}_{11}$ [m²/V²]	$10^{-7}\,n_2$ [W⁻¹]	$10^{-21}\,c_{11}$ [m²/V²]	Relative error ϵ [%]
[40]	72.3%	2.4	0.61	2.94	0.63	3.5
[41]	87.3%	3.1±0.4	0.89±0.12	2.82	0.90±0.12	1.2
[44]	88.6%	2.61	0.73	2.680	0.75	1.8

into two parts, one for the cladding and one for the waveguide. The total effective Kerr coefficient is a sum of the contributions stemming from both the waveguide core and the cladding:

$$n_2 = \frac{3c\varepsilon_0}{4N^2}\left(\Sigma_{\mathrm{wg}} + \Sigma_{\mathrm{clad}}\right), \tag{35}$$

with:

$$\Sigma_{\mathrm{wg}} \equiv \iint_{\mathrm{wg}} \left(C_{\mathrm{wg}}\vec{v}\right)\cdot\vec{e}^*\,\mathrm{d}x\,\mathrm{d}y, \tag{36a}$$

and:

$$\Sigma_{\mathrm{clad}} \equiv \iint_{\mathrm{clad}} \left(C_{\mathrm{clad}}\vec{v}\right)\cdot\vec{e}^*\,\mathrm{d}x\,\mathrm{d}y. \tag{36b}$$

The electric mode profiles $\vec{e}$ are obtained from mode simulation, from which the effective area is also found. Using existing values of c_{11} for SiO_2 of 0.389×10^{-22} m²/V² [45], c_{11} for Si_3N_4 can be found. See Section 10 in Supplement 1 for a numerical example.

All three waveguides are designed for the fundamental TE mode and have waveguide confinement between 72-89%, with the evanescent field extending into the SiO_2 cladding, and for [44] into the air top cladding. As an example, the simulated mode profile of the waveguide from [40] is plotted in Figure 3.

The tensor element found from each literature source, from both formalisms, can be found in Table 1, along with the relative error, found similarly to (22). The resulting mean c_{11} tensor

element for Si_3N_4 is:

$$c_{11} = 0.76 \times 10^{-21} \, \text{m}^2/\text{V}^2. \tag{37}$$

Not all studies provided uncertainties for their measurements preventing error estimation. The variations in values can be a result of the different manufacturing processes used, as the flow ratio during chemical vapor deposition (CVD) has been shown to modify the stoichiometry of Si_3N_4 films resulting in differing nonlinear tensor element values [46, 47]. The high uncertainty on the measurements from [41], and the resulting high uncertainties found for the nonlinear tensor elements, are also seen in other materials, such as barium borate (BBO) [48].

4. Discussion

The presented NLS equation for integrated photonics differs from the currently accepted derivations in multiple aspects. In particular, it avoids a series of assumptions on the electric field such as plane wave propagation and the magnitude of the longitudinal component along $\hat{z}$. Both are in contradiction to the purely imaginary z component seen in the mode simulation in Fig. 3. The model is not derived phenomenologically by assuming the existence of the Kerr effect, but is instead directly from Maxwell's equations. The model is derived with heterogenous waveguides in mind, allowing for dispersion and nonlinear contributions from multiple materials. It does not make assumptions on the magnitude of the nonlinear effects and with the derivation using the complex wavenumber $\vec{k}$ it includes a finite value of attenuation through the entire derivation. The inclusion gives insight into how it affects nonlinear mode coupling, with a clear dependence seen in the nonlinear term in (15) (first term on the right-hand side). This makes the model better suited in situations with high propagation loss, such as lasing near an optical bandgap or at shorter wavelengths. Nonlinear effects such as two-photon absorption, stimulated Raman scattering, and stimulated Brillouin scattering are not explicitly included in the derivation on the NLS equation, but could, along with other nonlinear effects, be included in $\vec{\mathcal{P}}^{(\text{NL})}$ in the chief equation, (8), or in the attenuation coefficient.

As the presented explicit formula for the group index, (20), shows good coincidence with the conventional expression, (21), our confidence in the validity of the presented formalism is very high. Having an explicit formula for the group index, and therefore GVD, provides more insights into how to engineer these quantities to desired values, e.g. normal or anomalous dispersion.

In integrated optics, the intensity across the waveguide cross-section varies greatly, resulting in an ill-defined quantity. Having the optical Kerr effect expressed by optical power is preferred as mode simulation software is readily available, and power is usually known in a laboratory setting, enabling quick calculations. This model excels when working with heterogeneous waveguides such as the quickly developing lithium niobate-on-silicon nitride platform [42]. Here a significant part of the mode profile leaks into the cladding/substrate and multiple materials with high nonlinearities are used. This leads to multiple contributions to the generated phase shift. The multiple contributions are in the presented model accounted for in (11) by splitting the integral into as many terms as there are nonlinear contributions. An example of this is provided in Supplement 1, section 10.

In the presented calculations in Section 3.1, a relative error in the third-order tensor element of 3.5% is found. This is in a well-guided mode with a waveguide confinement of 72.3%. The error will only increase for structures with lower waveguide confinement and a cladding material with a higher nonlinear coefficient. Using (8) to find coupled amplitude equations, as done for second harmonic generation in [27], the power of a generated signal scales with κ^2, escalating the significance of the error, and shows the importance of using the correct model for the task at hand.

Combined with the presented method for calculating c_{11}, the expression for the Kerr coefficient given in this paper will allow for better predictions in the design of devices utilizing the Kerr

effect, such as all-optical switches. The limiting factor for the accuracy of the model now becomes the large uncertainties in the C tensor elements, especially for non-amorphous materials with multiple independent tensor elements [48, 49].

5. Conclusion

This study introduces a novel formalism for describing nonlinear integrated photonics, derived from a generalized chief equation. The resulting nonlinear Schrödinger equation is applied to the case of degenerate four-wave mixing, revealing a bright soliton solution. The NLS equation is used to derive a more general formula for the group index, showing excellent coincidence with the conventional model. Moreover, the optical Kerr effect is expressed in terms of optical power, yielding a Kerr coefficient that depends explicitly on the waveguide mode and power. The application of this formalism is demonstrated by calculating the relevant nonlinear tensor coefficient for Si_3N_4. For one example this results in a relative error of 3.5% to the conventional model. By providing a rigorous derivation of the NLS equation this study helps model nonlinear effects in waveguides, but more research is necessary to gain insight into the overall scope of its implications especially in lossy materials. This could include simulations of the NLS equation in optical components such as long optical fibers, and ring resonators for frequency comb generation.

Funding

Disclosures

The authors declare no conflicts of interest.

Data avaibility

Data underlying the results presented in this paper are not publicly available at this time but may be obtained from the authors upon reasonable request.

Supplementary material

See Supplement 1 for supporting content.

References

1. Y. Kodama and A. Hasegawa, "Nonlinear pulse propagation in a monomode dielectric guide," IEEE J. Quantum Electron. **23**, 510–524 (1987).

2. B. Corcoran, M. Tan, X. Xu, A. Boes, J. Wu, T. G. Nguyen, S. T. Chu, B. E. Little, R. Morandotti, A. Mitchell, and D. J. Moss, "Ultra-dense optical data transmission over standard fibre with a single chip source," Nat. Commun. **11**, 2568 (2020).

3. H. Leopardi, J. Davila-Rodriguez, F. Quinlan, J. Olson, J. A. Sherman, S. A. Diddams, and T. M. Fortier, "Single-branch Er:fiber frequency comb for precision optical metrology with 10^{-18} fractional instability," Optica **4**, 879–885 (2017).

4. A. Schliesser, N. Picqué, and T. W. Hänsch, "Mid-infrared frequency combs," Nat. Photonics **6**, 440–449 (2012).

5. S. Ghanbari, R. Akbari, and A. Major, "Femtosecond Kerr-lens mode-locked alexandrite laser," Opt. Express **24**, 14836–14840 (2016).

6. F.-F. Du, G. Fan, X.-M. Ren, and M. Ma, "Deterministic hyperparallel control gates with weak Kerr effects," Adv. Quantum Technol. **6**, 2300201 (2023).

7. Y. Wang, C. F. Faurby, F. Ruf, P. I. Sund, K. Nielsen, N. Volet, M. J. Heck, N. Bart, A. D. Wieck, A. Ludwig *et al.*, "Deterministic photon source interfaced with a programmable silicon-nitride integrated circuit," NPJ Quantum Inf. **9**, 94 (2023).

8. X. Xue and N. Calabretta, "Nanosecond optical switching and control system for data center networks," Nat. Commun. **13**, 2257 (2022).

9. F. Ruf, L. Nielsen, N. Volet, and M. J. Heck, "Analysis and design of low-loss and fast all-optical switch elements on silicon nitride for integrated quantum photonics," J. Light. Technol. **40**, 7598–7609 (2022).

10. E. Lucas, S.-P. Yu, T. C. Briles, D. R. Carlson, and S. B. Papp, "Tailoring microcombs with inverse-designed, meta-dispersion microresonators," Nat. Photonics **17**, 943–950 (2023).

11. E. F. Perez, G. Moille, X. Lu, J. Stone, F. Zhou, and K. Srinivasan, "High-performance Kerr microresonator optical parametric oscillator on a silicon chip," Nat. Commun. **14**, 242 (2023).

12. D. T. Spencer, T. Drake, T. C. Briles, J. Stone, L. C. Sinclair, C. Fredrick, Q. Li, D. Westly, B. R. Ilic, A. Bluestone, N. Volet, T. Komljenovic, L. Chang, S. H. Lee, D. Y. Oh, M.-G. Suh, K. Y. Yang, M. H. P. Pfeiffer, T. J. Kippenberg, E. Norberg, L. Theogarajan, K. Vahala, N. R. Newbury, K. Srinivasan, J. E. Bowers, S. A. Diddams, and S. B. Papp, "An optical-frequency synthesizer using integrated photonics," Nature **557**, 81–85 (2018).

13. H. Bergeron, L. C. Sinclair, W. C. Swann, C. W. Nelson, J.-D. Deschênes, E. Baumann, F. R. Giorgetta, I. Coddington, and N. R. Newbury, "Tight real-time synchronization of a microwave clock to an optical clock across a turbulent air path," Optica **3**, 441–447 (2016).

14. E. Z. Ulsig, I. Degli-Eredi, E. J. Stanton, and N. Volet, "Efficient low threshold frequency conversion in AlGaAs-on-insulator waveguides," Front. Photon. **3**, 904651 (2022).

15. E. J. Stanton, P. Tønning, E. Z. Ulsig, S. Calmar, M. A. Bourland, S. T. Thomsen, K. B. Gravesen, P. Johansen, and N. Volet, "Continuous-wave second-harmonic generation in the far-uvc pumped by a blue laser diode," arXiv, 2309.04554 (2023).

16. J. M. Dudley, G. Genty, and S. Coen, "Supercontinuum generation in photonic crystal fiber," Rev. Mod. Phys. **78**, 1135 (2006).

17. V. N. Serkin and A. Hasegawa, "Novel soliton solutions of the nonlinear Schrödinger equation model," Phys. Rev. Lett. **85**, 4502 (2000).

18. Y. Shen, *The Principles of Nonlinear Optics* (Wiley, 1984).

19. R. W. Boyd, *Nonlinear Optics* (Academic Press, 2020).

20. P. S. Kuo and M. Fejer, "Mixing of polarization states in zincblende nonlinear optical crystals," Opt. Express **26**, 26971–26984 (2018).

21. T. J. Kippenberg, A. L. Gaeta, M. Lipson, and M. L. Gorodetsky, "Dissipative Kerr solitons in optical microresonators," Science **361**, eaan8083 (2018).

22. A. Boes, B. Corcoran, L. Chang, J. Bowers, and A. Mitchell, "Status and potential of lithium niobate on insulator (LNOI) for photonic integrated circuits," Laser Photonics Rev. **12**, 1700256 (2018).

23. G. Poberaj, H. Hu, W. Sohler, and P. Günter, "Lithium niobate on insulator (LNOI) for micro-photonic devices," Laser Photonics Rev. **6**, 488–503 (2012).

24. X. Han, M. Yuan, H. Xiao, G. Ren, T. G. Nguyen, A. Boes, Y. Su, A. Mitchell, and Y. Tian, "Integrated photonics on the dielectrically loaded lithium niobate on insulator platform," J. Opt. Soc. Am. B **40**, D26–D37 (2023).

25. G. P. Agrawal, *Nonlinear fiber optics* (Springer, 2019), 6th ed.

26. M. L. Madsen, E. Z. Ulsig, S. Folsach, P. H. Godoy, E. J. Stanton, and N. Volet, "Mid-infrared difference-frequency generation in AlGaAs-on-insulator waveguides," J. Opt. Soc. Am. B **40**, 1742–1748 (2023).

27. M. T. Hansen, E. Z. Ulsig, F. Labbé, M. L. Madsen, Y. Ding, K. Rottwitt, and N. Volet, "Efficient and robust second-harmonic generation in thin-film lithium niobate using modal phase matching," Front. Photon. **4**, 1324648 (2023).

28. Z. Zhu and T. G. Brown, "Full-vectorial finite-difference analysis of microstructured optical fibers," Opt. Express **10**, 853–864 (2002).

29. G. I. Stegeman and C. T. Seaton, "Nonlinear integrated optics," J. Appl. Phys. **58**, R57–R78 (1985).

30. X.-l. Yang and S.-w. Xie, "Expression of third-order effective nonlinear susceptibility for third-harmonic generation

in crystals," Appl. Opt. **34**, 6130–6135 (1995).

31. P. S. Banks, M. D. Feit, and M. D. Perry, "High-intensity third-harmonic generation," J. Opt. Soc. Am. B **19**, 102–118 (2002).
32. A. Hasegawa and F. Tappert, "Transmission of stationary nonlinear optical pulses in dispersive dielectric fibers. i. anomalous dispersion," Appl. Phys. Lett. **23**, 142–144 (1973).
33. M. Nakazawa, "Soliton transmission in telecommunication networks," IEEE Commun. Mag. **32**, 34–41 (1994).
34. T. Herr, V. Brasch, J. D. Jost, C. Y. Wang, N. M. Kondratiev, M. L. Gorodetsky, and T. J. Kippenberg, "Temporal solitons in optical microresonators," Nat. Photonics **8**, 145–152 (2014).
35. A. Jørgensen, D. Kong, M. Henriksen, F. Klejs, Z. Ye, Ò. Helgason, H. Hansen, H. Hu, M. Yankov, S. Forchhammer *et al.*, "Petabit-per-second data transmission using a chip-scale microcomb ring resonator source," Nat. Photonics **16**, 798–802 (2022).
36. Y. S. Kivshar and B. Luther-Davies, "Dark optical solitons: physics and applications," Phys. Rep. **298**, 81–197 (1998).
37. H. Danielmeyer and H. Weber, "Direct measurement of the group velocity of light," Phys. Rev. A **3**, 1708 (1971).
38. C. A. Barrios, B. Sánchez, K. B. Gylfason, A. Griol, H. Sohlström, M. Holgado, and R. Casquel, "Demonstration of slot-waveguide structures on silicon nitride/silicon oxide platform," Opt. Express **15**, 6846–6856 (2007).
39. B. Zabelich, E. Nitiss, A. Stroganov, and C.-S. Bres, "Linear electro-optic effect in silicon nitride waveguides enabled by electric-field poling," ACS Photonics **9**, 3374–3383 (2022).
40. K. Ikeda, R. E. Saperstein, N. Alic, and Y. Fainman, "Thermal and Kerr nonlinear properties of plasma-deposited silicon nitride/silicon dioxide waveguides," Opt. Express **16**, 12987–12994 (2008).
41. C. J. Krückel, A. Fülöp, Z. Ye, P. A. Andrekson *et al.*, "Optical bandgap engineering in nonlinear silicon nitride waveguides," Opt. Express **25**, 15370–15380 (2017).
42. M. Churaev, R. N. Wang, A. Riedhauser, V. Snigirev, T. Blésin, C. Möhl, M. H. Anderson, A. Siddharth, Y. Popoff, U. Drechsler *et al.*, "A heterogeneously integrated lithium niobate-on-silicon nitride photonic platform," Nat. Commun. **14**, 3499 (2023).
43. A. W. Elshaari, W. Pernice, K. Srinivasan, O. Benson, and V. Zwiller, "Hybrid integrated quantum photonic circuits," Nat. photonics **14**, 285–298 (2020).
44. Y. Qu, J. Wu, Y. Yang, Y. Zhang, Y. Liang, H. El Dirani, R. Crochemore, P. Demongodin, C. Sciancalepore, C. Grillet *et al.*, "Enhanced four-wave mixing in silicon nitride waveguides integrated with 2D layered graphene oxide films," Adv. Opt. Mater. **8**, 2001048 (2020).
45. B. Buchalter and G. R. Meredith, "Third-order optical susceptibility of glasses determined by third harmonic generation," Appl. Opt. **21**, 3221–3224 (1982).
46. C. J. Krückel, A. Fülöp, T. Klintberg, J. Bengtsson, P. A. Andrekson *et al.*, "Linear and nonlinear characterization of low-stress high-confinement silicon-rich nitride waveguides," Opt. Express **23**, 25827–25837 (2015).
47. T. Wang, D. K. Ng, S.-K. Ng, Y.-T. Toh, A. K. Chee, G. F. Chen, Q. Wang, and D. T. Tan, "Supercontinuum generation in bandgap engineered, back-end CMOS compatible silicon rich nitride waveguides," Laser Photonics Rev. **9**, 498–506 (2015).
48. M. Bache, H. Guo, B. Zhou, and X. Zeng, "The anisotropic Kerr nonlinear refractive index of the beta-barium borate (β-BaB$_2$O$_4$) nonlinear crystal," Opt. Mater. Express **3**, 357–382 (2013).
49. E. Dremetsika, B. Dlubak, S.-P. Gorza, C. Ciret, M.-B. Martin, S. Hofmann, P. Seneor, D. Dolfi, S. Massar, P. Emplit *et al.*, "Measuring the nonlinear refractive index of graphene using the optical Kerr effect method," Opt. Lett. **41**, 3281–3284 (2016).